





ORIGINAL ARTICLE

Parcellation of the Human Cerebral Cortex Based on Molecular Targets in the Serotonin System Quantified by Positron Emission Tomography *In vivo*

Gregory M. James ^{1,†}, Gregor Gryglewski ^{1,†}, Thomas Vanicek¹, Neydher Berroterán-Infante ², Cécile Philippe², Alexander Kautzky¹, Lukas Nics², Chrysoula Vraka², Godber M. Godbersen¹, Jakob Unterholzner¹, Helen L. Sigurdardottir¹, Marie Spies¹, René Seiger¹, Georg S. Kranz^{1,3}, Andreas Hahn¹, Markus Mitterhauser^{2,4}, Wolfgang Wadsak^{2,5}, Andreas Bauer⁶, Marcus Hacker², Siegfried Kasper¹ and Rupert Lanzenberger ¹


¹Department of Psychiatry and Psychotherapy, Medical University of Vienna, Vienna 1090, Austria,

²Department of Biomedical Imaging and Image-guided Therapy, Division of Nuclear Medicine, Medical

University of Vienna, Vienna 1090, Austria, ³Department of Rehabilitation Sciences, The Hong Kong Polytechnic University Hong Kong 999077, China, ⁴Ludwig Boltzmann Institute Applied Diagnostics, Vienna

1090, Austria, ⁵Center for Biomarker Research in Medicine (CBmed), Graz 8010, Austria and ⁶Institute of Neuroscience and Medicine (INM-2), Research Centre Jülich, Jülich 52428, Germany

[†]The first two authors contributed equally to this work.

Address correspondence to Prof. Rupert Lanzenberger, MD, PD, NEUROIMAGING LABS (NIL) - PET, MRI, EEG, TMS & Chemical Lab Department of Psychiatry and Psychotherapy, Medical University of Vienna, Waehringer Guertel 18-20, 1090 Vienna, AUSTRIA. Email: rupert.lanzenberger@meduniwien.ac.at  orcid.org/0000-0003-4641-9539

Abstract

Parcellation of distinct areas in the cerebral cortex has a long history in neuroscience and is of great value for the study of brain function, specialization, and alterations in neuropsychiatric disorders. Analysis of cytoarchitectonical features has revealed their close association with molecular profiles based on protein density. This provides a rationale for the use of *in vivo* molecular imaging data for parcellation of the cortex with the advantage of whole-brain coverage. In the current work, parcellation was based on expression of key players of the serotonin neurotransmitter system. Positron emission tomography was carried out for the quantification of serotonin 1A (5-HT_{1A}, *n* = 30) and 5-HT_{2A} receptors (*n* = 22), the serotonin-degrading enzyme monoamine oxidase A (MAO-A, *n* = 32) and the serotonin transporter (5-HTT, *n* = 24) in healthy participants. Cortical protein distribution maps were obtained using surface-based quantification. Based on k-means clustering, silhouette criterion and bootstrapping, five distinct clusters were identified as the optimal solution. The defined

clusters proved of high explanatory value for the effects of psychotropic drugs acting on the serotonin system, such as antidepressants and psychedelics. Therefore, the proposed method constitutes a sensible approach towards integration of multimodal imaging data for research and development in neuropharmacology and psychiatry.

Key words: cortex, cortical reconstruction, molecular imaging, parcellation, PET, serotonin

Introduction

The classification of the cerebral cortex into discrete regions bears several advantages for the study of brain function. Ideally, the distinction of parcels is reproducible across individuals and laboratories, and accompanied by a nomenclature, such that specific scrutiny and scientific discourse is facilitated. Historically, Brodmann areas constitute the most prominent attempt in this direction and are based on Brodmann's observations of cytoarchitectural features of the cerebral cortex (Zilles and Amunts 2010). The advance of new technologies that allow for the measurement of different properties of human brain tissue has spurred attempts to improve parcellation. Especially in the field of brain imaging, a reliable reference system is indispensable (Amunts et al. 2014), as exemplified by the effort of Talairach-Tournoux to translate Brodmann areas into a standardized coordinate system (Talairach and Tournoux 1988). Based on macro-anatomical landmarks, this atlas was transformed into the widely used MNI template created from an average of a multitude of MRI scans, which resulted in a more accurate representation of the population's neuroanatomy (Chau and McIntosh 2005). Atlases based on averages of multiple subjects do not entirely accommodate inter-individual variation, especially if their alignment is based on macro-anatomical landmarks, such as gyrfication of the cortex (Desikan et al. 2006; Destrieux et al. 2010), as these do not necessarily coincide with cytoarchitectural borders (Uylings et al. 2005). One promising solution has been proposed and validated using data from the human connectome project, which entails the acquisition of standardized structural and functional MR sequences for each subject and enables an individualized delineation of cortical areas using a machine-learning classifier (Glasser et al. 2016). Another invaluable approach is the construction of probabilistic cytoarchitectural atlases derived from computational analysis of histological sections in a set of several brains (Eickhoff et al. 2005). The finding that inter-individual variations in functional MRI activation could be reduced by representing the cerebral cortex in a two-dimensional coordinate system has initiated the trend of surface-based analysis (Fischl, Sereno, and Dale 1999; Fischl, Sereno, Tootell, et al. 1999). The benefits of this methodology have led to its extensive application in processing of structural and functional MRI, as well as molecular imaging data (Greve et al. 2014) and the investigation of structural and functional connectivity.

In the domain of connectivity analysis, the identification of parcels using resting-state fMRI signal and graph theoretical (Power et al. 2011), independent component (Yeo et al. 2014), Markov random field (Schaefer et al. 2017), or spectral clustering analysis (Craddock et al. 2012) has yielded appealing results with regard to reproducibility and elucidation of information processing in the cerebral cortex. On the other hand, hierarchical clustering approaches to parcellation may parallel the development of specialization in the cerebral cortex, as demonstrated in structural connectivity data (Moreno-Dominguez et al. 2014). A MRI study in twins which delineated clusters based solely on the heritability of cortical surface area similarly revealed a hierarchical organization of cortical areas (Chen

et al. 2013). Other invaluable approaches are derived from the analysis of functional connectivity networks in comparison to gene expression patterns (Ganglberger et al. 2017).

It could be argued that the field of parcellation of the cortex has undergone a gradual paradigm shift from dissecting maximally distinct areas towards the identification of the topology of coexisting sub-systems. Interestingly, borders between regions defined by cytoarchitectural features were found to coincide to a great extent with those defined by receptor profiles using autoradiography (Zilles et al. 2002), suggesting that functional differentiation of the cerebral cortex may be paralleled by receptor compositions. Not only does this constitute complementary information and render multimodal support for the parcellation derived from cytoarchitectonics, but it provides a rationale for the utilization of molecular imaging data *in vivo* to study brain ontology. A linear relationship between protein densities measured using autoradiography and outcome measures derived from molecular imaging methods such as positron emission tomography (PET) has been demonstrated for several proteins (Savli et al. 2012; Beliveau et al. 2017). A critical advantage of molecular imaging is that acquisition of comprehensive whole-brain data is possible within a single scan, as opposed to effortful sectioning and staining of selected regions. We therefore propose clustering using PET imaging data of molecular targets as a complementary approach to parcellation of the cortical surface. We expect that clusters defined on the expression of molecular targets will be of special relevance for the analysis of pharmacological imaging data and therefore facilitate research and development in this field. The presented analysis is constrained to PET data on four proteins involved in serotonergic neurotransmission for which a representative sample is available. Inarguably the serotonergic system exerts a strong influence during brain development, modulation of a large set of brain functions and behavior, and is one of the most important targets of therapeutic intervention in neuropsychopharmacology. Extensive application of the proposed parcellation methods to different neurotransmitter systems can be expected with the emergence of data sharing initiatives in the molecular imaging field (Knudsen et al. 2016). The resulting clusters were compared to established cytoarchitectonic and functional brain parcellations and interpreted in light of pharmacological effects targeting the investigated binding proteins.

Materials and Methods

Participants and Imaging Procedures

The dataset used in this analysis comprises PET and structural 3T MR measurements of 108 healthy participants in total. Each subject underwent one PET scan for one target. For details on demographics and data acquisition see Table 1, or previous publications covering the data used here (Elmenhorst et al. 2012; Lanzenberger et al. 2007, 2012; Gryglewski et al. 2017; Vanicek et al. 2017). Subjects were recruited by advertisement

Table 1 Data composition, demographics and acquisition parameters.

Protein	5-HT _{1A} receptor	5-HT _{2A} receptor	MAO-A	5-HTT
Radioligand	[carbonyl- ¹¹ C]WAY-100635	[¹⁸ F]altanserin	[¹¹ C]harmine	[¹¹ C]DASB
Outcome measure	BP _{ND}	BP _p	V _T	BP _{ND}
N (females)	30 (14)	22 (16)	32 (17)	24 (7)
Age (mean ± SD)	26.7 ± 6.8	40.7 ± 11.6	35.3 ± 10.5	29.4 ± 8.0
PET scanner (3D mode)	GE Advance PET scanner	Siemens ECAT Exact HR+ scanner	GE Advance PET scanner	GE Advance PET scanner
Tracer administration	Bolus	Bolus plus infusion (K _{bol} = 2.1 h)	Bolus	Bolus
Dynamic emission scan	90 min	60 min (starting 120 min after tracer bolus)	90 min	90 min
Blood samples	—	venous	arterial	—
MRI (T1-weighted structural images)	Bruker Medspec 3T, MPRAGE: voxel size 0.78 × 0.86 × 1.56 mm	Siemens Magnetom Trio 3T, MPRAGE: 1 × 1 × 1 mm	Siemens Tim Trio 3 T(n = 15): 0.88 × 0.47 × 0.47 mm; Siemens PRISMA 3 T(n = 17): 1.1 × 1 × 1 mm	Bruker Medspec 3 T (n = 3), MPRAGE: 0.78 × 0.86 × 1.56 mm; Philips Achieva 3 T(n = 11), FFE: 0.88 × 0.47 × 0.47 mm; Siemens mMR 3 T(n = 10), MPRAGE: 1.1 × 1 × 1 mm

PET and MRI data from a total of 108 healthy subjects was obtained for the current analysis.

and provided written informed consent according to the study procedures approved by the Ethics Committees at the Medical University of Vienna, Austria, and the Medical Faculty of the University of Düsseldorf, Germany. Participants underwent medical examinations to assure their physical and mental health. Subjects had no history of psychopharmacological drug treatment, substance abuse or diagnosis of psychiatric conditions according to the Diagnostic and Statistical Manual of Mental Disorders IV (DSM-IV). Scans were performed regardless of menstrual cycle of female participants.

PET imaging was carried out using optimized protocols with application of highly specific tracers for quantification of the 5-HT_{1A} receptor ([carbonyl-¹¹C]WAY-100635), 5-HT_{2A} receptor ([¹⁸F]altanserin), MAO-A ([¹¹C]harmine) and serotonin transporter 5-HTT ([¹¹C]DASB). [carbonyl-¹¹C]WAY-100635 has a tenfold lower affinity for dopamine D4 receptors than for 5-HT_{1A} receptors (Chemel et al. 2006; Martel et al. 2007). Based on the low expression of D4 receptor mRNA in the cortex, we do not expect a relevant influence on binding potentials in this region (Matsumoto et al. 1996). Changes in [¹¹C]harmine binding up to 17% were observed in one study after altering endogenous monoamine concentrations pharmacologically (Sacher et al. 2012). The other tracers used were shown to be insensitive to changes in endogenous ligand concentrations, with changes in [¹¹C]DASB binding being observed only after extreme pharmacological challenges performed in animal studies (Paterson et al. 2010).

Image Preprocessing

PET images were motion corrected in SPM12 (Wellcome Trust Centre for Neuroimaging, London, UK; <http://www.fil.ion.ucl.ac.uk/spm>) by rigid realignment of every frame image to a median image, which consisted of a motion-free period, selected by visual inspection. Duration of frames were between 5 and 300 s, depending on the protocol and time point (frame length was increasing towards the end of the measurements to improve signal to noise ratio). The median PET images were co-registered to the individual MR images. The cortical surface was reconstructed using FreeSurfer 6.0 (Harvard Medical School, Boston, USA; <http://www.surfer.nmr.mgh.harvard.edu>)

with individual T1-weighted MR images serving as input. In addition, every reconstruction was visually inspected and manually corrected for possible inaccuracies in segmentation of the cortical surface by setting control points or erasing falsely segmented areas and re-initiating reconstruction according to published procedures (McCarthy et al. 2015). Volume to surface projection was performed using the FreeSurfer function *mri_vol2surf*. The obtained registration parameters were subsequently applied to the motion-corrected dynamic PET images resulting in dynamic PET data in fsaverage surface space.

Quantification of Molecular Targets

The dynamic PET data registered to the cortical surface served as input for the quantification of protein distributions, which was performed in MATLAB 8.2 (<https://www.mathworks.com>) using models specified below. PET data was smoothed prior to quantification using an 8-mm kernel in surface space. The resulting outcome measures (binding potential, BP_{ND}, BP_p, V_T) are proportional to absolute density of available receptors (Innis et al. 2007).

5-HT_{1A} Receptor

The cortical 5-HT_{1A} receptor binding was quantified by applying the multilinear reference tissue model (MRTM2) (Ichise et al. 2003). The insular cortex was used as high-uptake and the cerebellar white matter as reference region, due to the low 5-HT_{1A} concentration in this area (Parsey et al. 2005). The choice of quantification method for 5-HT_{1A} receptor binding potentials may affect results of group comparisons based on variability of receptors in the reference region (Parsey et al. 2010). This issue is not relevant to the current analysis, as a potentially different scaling of data is removed by normalization prior to clustering.

5-HT_{2A} Receptor

5-HT_{2A} receptor binding potential (BP_p) was quantified using radioactivity in brain and blood plasma at equilibrium during tracer infusion (Elmenhorst et al. 2012). Activity in the reference

region (cerebellum) was subtracted from cortical activity and divided by plasma activity.

Serotonin Transporter

Modeling of 5-HTT binding was similar to that in previous publications (James et al. 2017). In brief, the MRTM2 was applied with thalamus serving as high-uptake and cerebellar gray matter as reference region to obtain the binding potential (BP_{ND} ; Parsey et al. 2006).

Monoamine Oxidase A

Arterial blood sampling was performed to obtain arterial input functions after correction for the presence of radioactive metabolites using high-performance liquid chromatography. Arterial input functions were derived from the kinetic modeling tool implemented in PMOD 3.509 (PMOD Technologies Ltd., Zurich, Switzerland; <http://www.pmod.com>). The arterial input functions and cortical activity were processed using Logan plots to obtain volume of distribution (V_T) as the outcome measure for MAO-A binding (Logan et al. 1990; Ginovart et al. 2006).

Clustering Method

For each protein, data was averaged across subjects resulting in population-based maps for the distribution of 5-HT_{1A} receptors, 5-HT_{2A} receptors, MAO-A and 5-HTT on the cortical surface. In order to avoid weighting in the parcellation procedure owing to the differently scaled outcome measures, binding data for each protein was z-scored, which resulted in values with a mean of 0 and a standard deviation of 1. The standardized mean maps for the four proteins were used as input for the k-means clustering algorithm. The initial starting values were chosen according to the K-means++ algorithm (Arthur and Vassilvitskii 2007). Clustering was performed with a squared Euclidean distance measure. The solution with the lowest within-cluster sums of point-to-centroid distances was selected from 50 replicates. To obtain a robust estimate of the optimal number of clusters, bootstrapping was performed using subsets of the PET data. One hundred subsets were generated by randomly selecting five subjects for each molecular target. For each subset, the optimal number of clusters was determined by the silhouette criterion using squared Euclidean distance (Rousseeuw 1987). Possible K were evaluated from 4 (corresponding to the number of proteins used for clustering) to a limit of 20, due to the tendency of the criterion values to decrease with an increasing number of clusters. The K indicated for the majority of subsets in bootstrapping was selected as the optimal solution for the entire dataset. While selection of the optimal number of clusters was performed on a combined dataset of both hemispheres for computational reasons, clustering of the entire dataset was performed both for each hemisphere separately and on a combined dataset of both hemispheres.

To evaluate the resulting clusters, we examined the overlap of parcellation based on serotonergic molecules with those of the population-average, landmark- and surface-based version of the Brodmann atlas (Van Essen 2005), as well as a cortical parcellation based on major functional connectivity networks (Yeo et al. 2011).

Results

Cortical protein maps generated for 5-HT_{1A} receptors, 5-HT_{2A} receptors, MAO-A and 5-HTT were in good agreement with distributions reported in the literature (Figure 1, Table 2) (Varnas et al.

2004; Savli et al. 2012; Beliveau et al. 2017). The silhouette criterion indicated K = 5 as the optimal solution in 83 out of 100 subsets during bootstrapping. As results for combined and separate analysis of hemispheres were highly similar (Supplementary Figure 1), the subsequent paragraphs only refer to results of the combined analysis. The topology and molecular profiles of clusters are shown in Figure 2 and Table 2. The comparison with other cortical parcellation methods is shown in Figure 3 and Supplementary Table 1. Supplementary Figure 2 displays multiple perspectives of clustering results. Clustering results are available for download in NIfTI and FreeSurfer (.annot) file formats at <http://www.meduniwien.ac.at/neuroimaging/parcellation.html>. Properties of clusters are summarized in the following paragraphs. Numbering of the clusters is arbitrary.

Cluster 1

Cluster 1 has the lowest binding of MAO-A, 5-HT_{1A}, and 5-HT_{2A} receptors. The majority of its area is located on the pre- and postcentral gyri and the paracentral lobule and extends to the superior parietal gyrus. Another part can be found adjacent to the corpus callosum extending from the caudal anterior cingulate cortex to the retrosplenial isthmus cingulate cortex and parahippocampal gyrus (Brodmann areas (BA) 26-29 and 35). Almost two-thirds of this cluster correspond to the somatomotor network and comprise the majority of BA 1-5, 6, and 7.

Cluster 2

Cluster 2 is characterized by the highest binding of excitatory 5-HT_{2A} receptors among all clusters and second highest expression of inhibitory 5-HT_{1A} receptors. The cluster spans 24% of the cortical surface. Two-thirds of the cluster are located in the superior, middle and inferior temporal gyri (BA 20-22 which contain Wernicke's speech area), and extend to adjacent lateral occipital, fusiform (BA 37), angular, supramarginal, inferior parietal gyri (BA 39, 40). The remaining part of the cluster is located in the frontal cortex and comprises the majority of the rostral middle frontal gyrus (BA 9, 10, 46). Approximately 10% of the cluster are located in the medial and lateral orbitofrontal cortex (BA 11) and extend into the medial aspect of the superior frontal gyrus. Cluster 2 covers 30% of the default and 43% of the limbic networks.

Cluster 3

Cluster 3 is the largest cluster and includes 37% of the cortical surface. Binding of 5-HTT is the lowest among all clusters, 5-HT_{1A} receptors and MAO-A are below average. One half of the cluster is located in the superior and inferior parietal cortex and extends into the precuneus (BA 7), lateral occipital (BA 19), supramarginal, and postcentral gyri. The remainder of the cluster can be found in the superior frontal gyrus (BA 8, 9) and covers the majority of the middle and inferior frontal (BA 45-47) gyri, as well as parts of the lateral orbitofrontal cortex and precentral gyrus (BA 6). Cluster 3 contributes 60% each to the dorsal attention and frontoparietal networks, and 40% each to the default mode and visual networks.

Cluster 4

Cluster 4 has the highest binding of MAO-A and the second highest binding of 5-HTT. Binding of 5-HT_{2A} and 5-HT_{1A} receptors is slightly above and below average, respectively. The majority of Cluster 4 is located on the medial aspect of the cortex, spans from

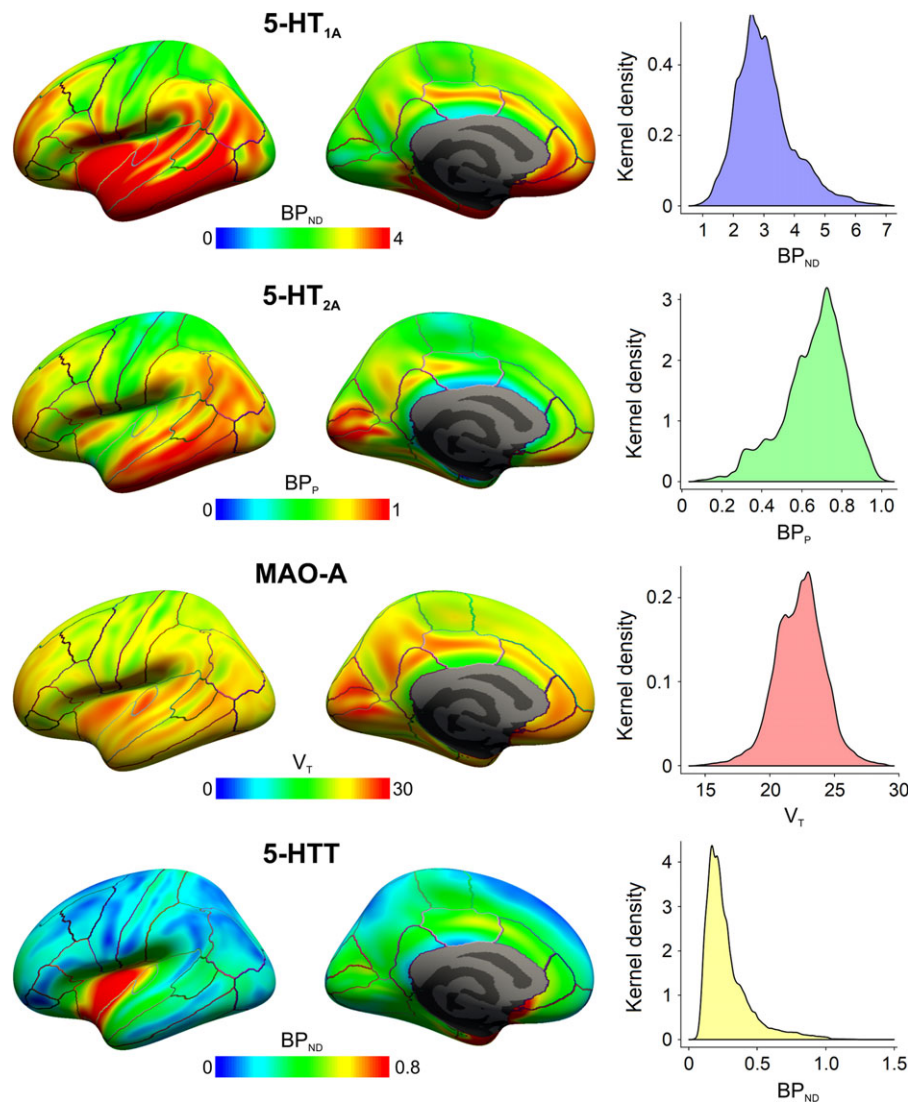


Figure 1. Population-based cortical protein binding maps. PET data on expression of four proteins centrally involved in modulatory serotonergic neurotransmission in the cerebral cortex is displayed. An inflated representation of the cortical surface is shown from a lateral (left) and mid-sagittal (middle) perspective. Kernel density plots illustrate the distribution of protein binding data in the average cortex (right). The kernel density is proportional to the number of data points at each value. Outcome measures (binding potentials (BP_{ND} or BP_p) or volume of distribution (V_T)) are proportional to absolute density of available protein. A total of 108 subjects were investigated, such that 22–32 individual scans were averaged to obtain each protein map.

Table 2 Protein binding profiles of molecular clusters.

	5-HT _{1A} receptor (BP_{ND})	5-HT _{2A} receptor (BP_p)	MAO-A (V_T)	5-HTT (BP_{ND})	Surface (%)
Cortical surface	3.04 ± 0.93	0.66 ± 0.16	22.30 ± 1.92	0.28 ± 0.17	100
Cluster 1	2.16 ± 0.48	0.43 ± 0.10	19.86 ± 1.40	0.23 ± 0.10	19.15
Cluster 2	3.86 ± 0.55	0.81 ± 0.07	23.52 ± 0.82	0.26 ± 0.08	23.86
Cluster 3	2.74 ± 0.40	0.67 ± 0.07	21.69 ± 0.87	0.19 ± 0.07	36.96
Cluster 4	2.70 ± 0.61	0.72 ± 0.11	24.48 ± 1.49	0.40 ± 0.10	12.71
Cluster 5	4.81 ± 0.90	0.61 ± 0.16	24.04 ± 1.32	0.71 ± 0.16	7.32

Mean and standard deviation of outcome measures for each cluster and protein are given. Corresponding kernel density plots of standardized binding data are shown in Figure 2.

the rostral (BA 24, 33) to the posterior cingulate cortex (BA 23, 30, 31) and reaches into visual areas including the pre-transverse temporal gyri (BA 41, 42). Cluster 4 covers one-third of the visual and one-fifth of the default mode networks.

Cluster 5

The highest binding of 5-HT_{1A} receptors and 5-HTT can be found in Cluster 5, and binding of MAO-A is ranked second.

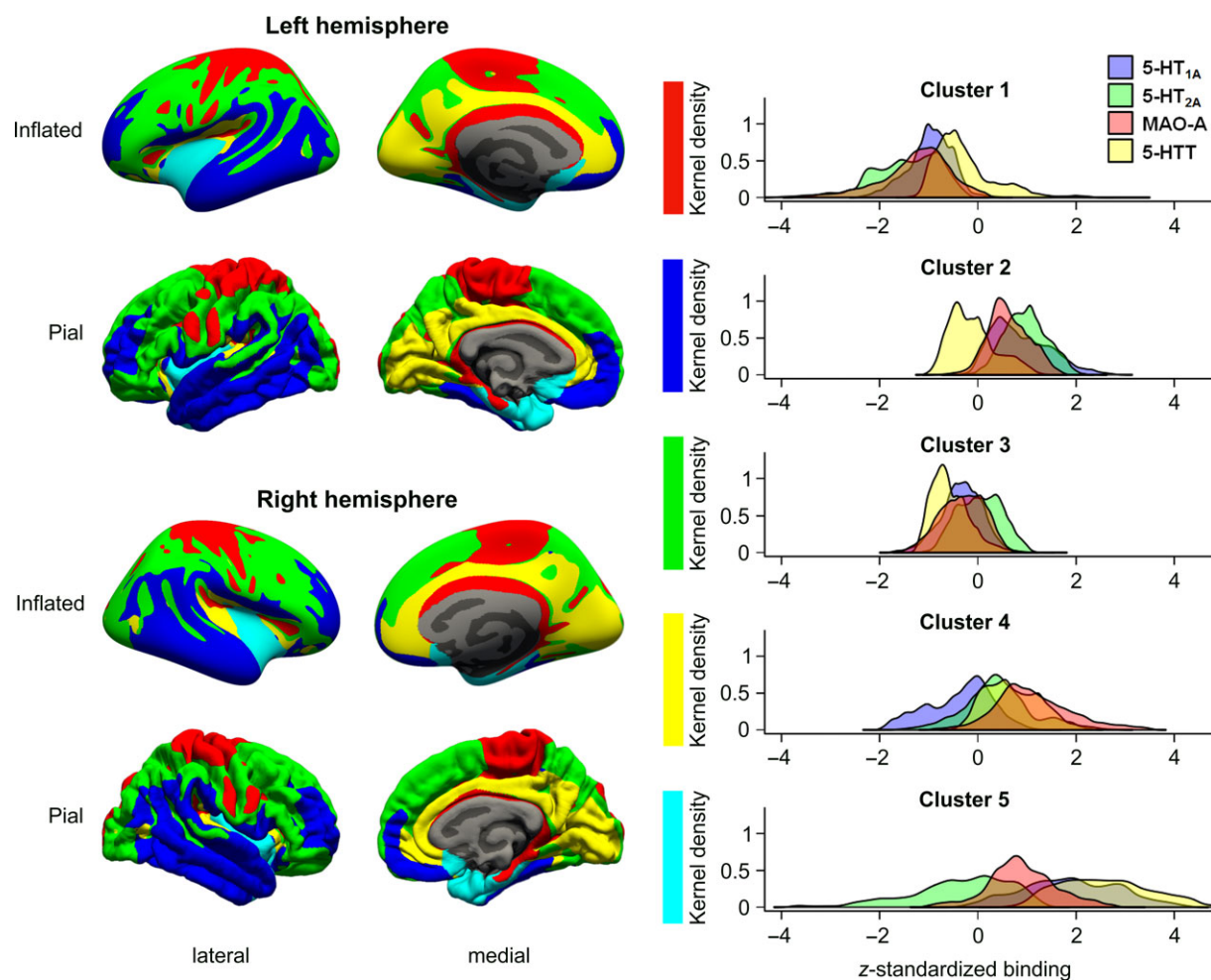


Figure 2. Topology and binding profiles of molecular clusters. Results of k-means clustering of cerebral cortex based on PET data of binding of 5-HT_{1A} and 5-HT_{2A} receptors, MAO-A and 5-HTT are summarized in this figure. The left and middle column display the allocation to one out of seven clusters for each coordinate on the cortical surface. Kernel density plots of standardized protein binding in each of the five clusters are shown in the right column. Corresponding absolute mean and standard deviations can be found in Table 2. Different perspectives on clustering results are displayed in Supplementary Figure 2.

This cluster is the smallest and encompasses most of the insula (BA 13-16), temporal pole (BA 38) and entorhinal cortex and reaches out to the parahippocampal, fusiform (BA 36), and superior temporal gyri. Furthermore, Cluster 5 has an extension into the posterior parts of the orbitofrontal cortex and includes the subgenual area (BA 25). Cluster 5 contributes to 42% of the limbic network.

Discussion

Relevance of Molecular Clusters in the Serotonergic System

The current results represent a proof of principle for the parcellation of the cerebral cortex based on the topology of serotonergic molecular targets measured using PET. The convergence of clustering results in separate and combined analysis of left and right hemispheres provides internal validation for the method and indicates that clusters identified are not subject to a pronounced influence of lateralization. While $k = 5$ is a relatively low number of clusters compared to the number of regions identified by cytoarchitectural features and the MR based methods discussed above, many of

the allocations of cortical areas are consistent in synopsis with other methods. It must be kept in mind that the current clustering approach is merely based on four parameters, i.e., four different proteins involved in the same neurotransmitter system, such that differentiation of regions is achieved with respect to the distribution of these particular molecules. It is likely that the inclusion of PET data on other proteins will result in a finer parcellation of cortical regions. Nevertheless, the unique characteristics of each cluster provide a novel perspective on the nature of serotonergic neuromodulation in the cerebral cortex and hint at the potential utility of the proposed parcellation for the investigation of pharmacological effects in this system. In fact, it may be a sensible approach to tailor regions of interests for the analysis of pharmacological imaging data using clustering based on expression of molecular targets of the studied drugs (Gryglewski et al. 2018). If brain areas within clusters defined in this manner react uniformly to pharmacological intervention, a substantial increase in power can be expected. Multiple comparisons can be avoided in contrast to analyses based on atlases obtained from other parcellation methods which may suggest distinctions between brain areas that are not paralleled by a differential response to the effects of the studied drug.

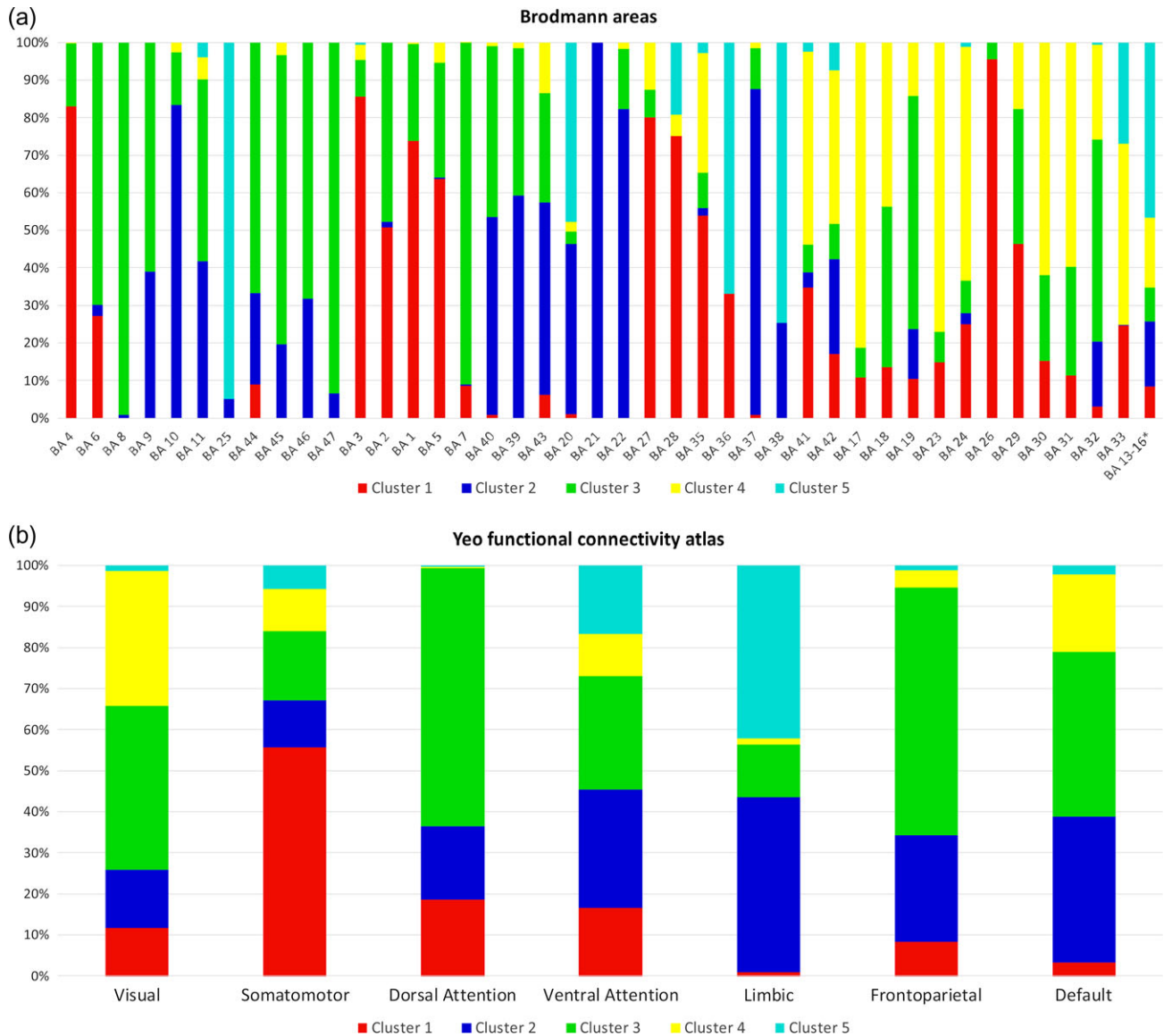


Figure 3. Overlap of molecular clusters with other cortical parcellation methods. The composition of region defined by different parcellation methods with respect to molecular clusters is displayed. For each region (x-axis), the fraction of the area allocated to each cluster is displayed as a bar summing to 100% on the y-axis. Regions were defined by (a) the cytoarchitectonical Brodmann areas (BA) and (b) the functional connectivity Yeo atlas. Complementary information on the distribution of each molecular cluster across regions defined by the other parcellation methods is shown in Supplementary table 1. *The Freesurfer version of the PALS Brodmann atlas misses the assignment of one area, which has a considerable overlap with the insular cortex. Thus, we summarized the unassigned region with Brodmann area 13-16 according to Brodmann and Garey (2006).

In detail, Cluster 1 is almost exclusively covered by the somatomotor network located at the pre- and postcentral gyrus and it may be argued that the proposed parcellation method failed to identify the indisputable border between primary motor and somatosensory cortices. However, if we consider that Cluster 1 is characterized by the lowest expression of all proteins studied, we may hypothesize that the effect of serotonergic neuromodulation is relatively low in these areas after completion of brain development (D'Amato et al. 1987). This is in line with the lack of effects on brain activation of 5-HT_{2A} receptor agonists in this area (Kraehenmann et al. 2015). The adjacent Cluster 3 is characterized by the lowest binding of serotonin transporters, the expression of which has been found to be highly associated with extracellular serotonin levels (Dewar et al. 1991). Higher binding of serotonin receptors

suggest that serotonergic neuromodulation may be effectuated in secondary and associative regions within Cluster 3, i.e. parts of the dorsal attention, frontoparietal, default mode and visual networks, at lower levels of serotonin or serotonin receptor binding drugs than in Cluster 1. Based on the low expression of 5-HTT, no pronounced effects of selective serotonin reuptake inhibitors (SSRIs) can be expected in clusters 1, 2, and 3. In contrast, Cluster 2 is characterized by relatively higher binding of MAO-A compared to 5-HTT and 30% and 43% of this cluster overlap with the default mode and limbic networks, respectively. These areas include the medial prefrontal cortex, temporoparietal junction, orbitofrontal cortex (Raichle and Snyder 2007; Sheline et al. 2009; Zhu et al. 2012), as well as the dorso-lateral prefrontal cortex which is targeted with transcranial magnetic stimulation for the treatment of depression

(Kolbinger et al. 1995; Pascual-Leone et al. 1996). This may underlie the response of patients to MAO inhibitors who have failed antidepressant treatment with SSRIs and justifies the independent role of the success of a trial with MAO inhibitors in staging of treatment resistant depression (Ruhe et al. 2012). The high expression of MAO-A in Cluster 4, 50% of which belongs to the visual network, may further underlie the increase of visual hallucinations with the addition of MAO inhibitors in the form of harmine (radiolabeled for the quantification of MAO-A in our study) and other harmala alkaloids to dimethyltryptamine in ayahuasca preparations, next to their influence on first-pass metabolism (McKenna et al. 1984; De Araujo et al. 2012). Given their high expression of 5-HT_{2A} receptors, Clusters 2 and 4 are implicated in the effects of drugs acting as agonists on these receptors, such as psilocybin and LSD, which is in line with psychedelic effects on visual and auditory perception and corresponding imaging studies on glucose metabolism, fMRI parameters and blood flow in these areas which were found to correlate with subjective drug effects (Vollenweider et al. 1997; Kraehenmann et al. 2015; Carhart-Harris et al. 2012, 2016). Lastly, with their high expression of 5-HTT Clusters 4 and 5 are most likely to be affected by the application of SSRIs which constitute the first line of treatment for depression and anxiety disorders. The extent of Cluster 4 in the cingulate and Cluster 5 in the parahippocampal and insular cortices includes regions that were historically assigned to the limbic system and are continuously under investigation for their role in emotion processing (Mayberg et al. 1999), empathy (Mitchell et al. 2013), and affective disorders (Montag et al. 2009; Horn et al. 2010; Klumpers et al. 2010). There is a remarkable overlap between these clusters and peak decreases in 5-HT_{1A} receptor binding following treatment with SSRIs (Spindelegger et al. 2009) or electroconvulsive therapy (Lanzenberger et al. 2013), and increases in gray matter volume following electroconvulsive therapy (Sartorius et al. 2016).

Limitations

Next to the limitation that only four proteins were available for the current analysis, several other issues should be mentioned. Given the resolution of molecular imaging using PET, some areas may be affected by partial volume effects, that is blurring of signal at borders between adjacent regions. While partial volume effects are reduced by surface-based analysis (Greve et al. 2014), some regions may be still affected and result in the identification of clusters in areas of mixed signal. The delineation of Cluster 1 close to the corpus callosum is likely due to a partial volume effect rather than low binding in this area of the cingulate cortex. The localization of proteins on pre- or post-synaptic sites, excitatory or inhibitory neurons cannot be differentiated using PET, but is likely to vary across the cortex and affect the effects of pharmacological modulation. Another issue is the fact that all four proteins could not be quantified in the same subjects, to the end that covariances between these proteins are unknown and probabilistic information on the inter-individual variation of the extent of clusters could not be generated. However, the protein maps in this analysis are generated from an adequately sized sample of healthy subjects and should constitute a fair representation of average protein distribution in the healthy adult population. Nevertheless, the study of the influence of demographic variables on clustering results cannot be performed with this sample size. The use of a different scanner for 5-HT_{2A} receptor imaging may reduce the conformity of resulting PET data, which may have been

accommodated by the uniform quantification pipeline, smoothing and standardization of the data. The focus of the current work was parcellation of the cortex. Clustering of cerebellum was not performed based on its negligible concentration of three out of four proteins studied, for the quantification of which it serves as reference region. Given the lack of a validated quantification pipeline which allows for integration of cortical surface-based outcome measures with volumetric subcortical regions, these would have to be processed separately. Furthermore, an optimized normalization pipeline for registration of PET data obtained from subcortical regions using different tracers is lacking. Lastly, at the present time we could only provide support for the utility of our method with reference to previous research in pharmacological imaging. Direct application of the defined clusters for analysis of imaging data is still pending.

Concluding Remarks

Definition of brain regions using clustering of molecular imaging data results in a parcellation of the cerebral cortex which is of high explanatory value for the appraisal of the effects of psychotropic drugs. The application of parcels defined in this manner for the analysis of pharmacological imaging data *a priori* will increase sensitivity and power of these investigations using, e.g. functional magnetic resonance imaging, which is a pressing issue in the field. Therefore, the proposed method constitutes a highly promising approach towards integration of multimodal imaging data for research and development in neuropharmacology and psychiatry.

Supplementary Material

Supplementary material is available at *Cerebral Cortex* online.

Funding

This work was supported by the Austrian Science Fund FWF (KLI504 and P27141 to L.R., KLI551 to S.K., and P24359 to Winkler D); the Else Kröner-Fresenius-Stiftung (2014_A192 to L.R.) and the Oesterreichische Nationalbank (11468 to L.R., 13675 to M.M., and 12809 to K.S.). G.G. is recipient of a DOC Fellowship of the Austrian Academy of Sciences at the Medical University of Vienna.

Notes

We thank Frey R., Winkler D., Winkler-Pjrek E., Baldinger-Melich P., Kraus C., Höflich A., Hienert M., Komorowski A., Silberbauer L., Traub-Weidinger T., Karanikas G., Moser U., Stein (Huf) P., Akimova E., Fink M. and Spindelegger C. for their medical assistance. Further, we thank the production staff of the Division of Nuclear Medicine, Department of Biomedical Imaging and Image-guided Therapy, i.e. Pichler V., Klebermass E., Haeusler D., and Mien L.K., for the synthesis of the radiotracers. We are grateful to Rischka L., Klöbl M., Ganger S., Handschuh P., Holik A. and Savli M. and for their technical, as well as Jungwirth J., Einenkel K., Cambioli L., Michenthaler P., Spurny B., Geiss-Granadia T. for their administrative support. Special thanks go to Kroll T., Elmenhorst D., and Matusch A. from Jülich, Germany, for their help on data transfer and processing. Last but not least, we are deeply indebted to the developers of the software Freesurfer (<http://www.surfer.nmr.mgh.harvard.edu>), especially to Greve D.N. and colleagues, who just recently implemented additional features to quantify PET

data on the cortical surface, a tool essential for processing of the study results presented here. This scientific project was performed with the support of the Medical Imaging Cluster of the Medical University of Vienna. *Conflict of Interest:* With relevance to this work there is no conflict of interest to declare.

References

- Amunts K, Hawrylycz MJ, Van Essen DC, Van Horn JD, Harel N, Poline JB, De Martino F, Bjaalie JG, Dehaene-Lambertz G, Dehaene S, et al. 2014. Interoperable atlases of the human brain. *Neuroimage*. 99:525–532.
- Arthur D, Vassilvitskii S. 2007. k-means++: the advantages of careful seeding. In: *Proceedings of the eighteenth annual ACM-SIAM symposium on Discrete algorithms*. p. 1027–1025.
- Beliveau V, Ganz M, Feng L, Ozenne B, Hojgaard L, Fisher PM, Svarer C, Greve DN, Knudsen GM. 2017. A high-resolution in vivo atlas of the human brain's serotonin system. *J Neurosci*. 37:120–128.
- Brodman K, Garey LJ. 2006. *Brodman's Localisation in the Cerebral Cortex*. New York (USA): Springer.
- Carhart-Harris RL, Erritzoe D, Williams T, Stone JM, Reed LJ, Colasanti A, Tyacke RJ, Leech R, Malizia AL, Murphy K, et al. 2012. Neural correlates of the psychedelic state as determined by fMRI studies with psilocybin. *Proc Natl Acad Sci USA*. 109:2138–2143.
- Carhart-Harris RL, Muthukumaraswamy S, Roseman L, Kaelen M, Droog W, Murphy K, Tagliazucchi E, Schenberg EE, Nest T, Orban C, et al. 2016. Neural correlates of the LSD experience revealed by multimodal neuroimaging. *Proc Natl Acad Sci USA*. 113:4853–4858.
- Chau W, McIntosh AR. 2005. The Talairach coordinate of a point in the MNI space: how to interpret it. *Neuroimage*. 25: 408–416.
- Chemel BR, Roth BL, Armbruster B, Watts VJ, Nichols DE. 2006. WAY-100635 is a potent dopamine D4 receptor agonist. *Psychopharmacology (Berl)*. 188:244–251.
- Chen CH, Fiecas M, Gutiérrez ED, Panizzon MS, Eyler LT, Vuoksima E, Thompson WK, Fennema-Notestine C, Hagler DJ, Jernigan TL, et al. 2013. Genetic topography of brain morphology. *Proc Natl Acad Sci USA*. 110:17089–17094. doi: 10.1073/pnas.1308091110.
- Craddock RC, James GA, Holtzheimer PE, Hu XP, Mayberg HS. 2012. A whole brain fMRI atlas generated via spatially constrained spectral clustering. *Hum Brain Mapp*. 33:1914–1928.
- De Araujo DB, Ribeiro S, Cecchi GA, Carvalho FM, Sanchez TA, Pinto JP, de Martinis BS, Crippa JA, Hallak JEC, Santos AC. 2012. Seeing with the eyes shut: neural basis of enhanced imagery following ayahuasca ingestion. *Hum Brain Mapp*. 33:2550–2560.
- Desikan RS, Ségonne F, Fischl B, Quinn BT, Dickerson BC, Blacker D, Buckner RL, Dale AM, Maguire RP, Hyman BT, et al. 2006. An automated labeling system for subdividing the human cerebral cortex on MRI scans into gyral based regions of interest. *Neuroimage*. 31:968–980.
- Destrieux C, Fischl B, Dale A, Hagren E. 2010. Automatic parcellation of human cortical gyri and sulci using standard anatomical nomenclature. *Neuroimage*. 53:1–15.
- Dewar KM, Reader TA, Grondin L, Descarries L. 1991. [3H] Paroxetine binding and serotonin content of rat and rabbit cortical areas, hippocampus, neostriatum, ventral mesencephalic tegmentum, and midbrain raphe nuclei region. *Synapse*. 9:14–26.
- D'Amato RJ, Blue ME, Largent BL, Lynch DR, Ledbetter DJ, Molliver ME, Snyder SH. 1987. Ontogeny of the serotonergic projection to rat neocortex: transient expression of a dense innervation to primary sensory areas. *Proc Natl Acad Sci USA*. 84:4322–4326.
- Eickhoff SB, Stephan KE, Mohlberg H, Grefkes C, Fink GR, Amunts K, Zilles K. 2005. A new SPM toolbox for combining probabilistic cytoarchitectonic maps and functional imaging data. *Neuroimage*. 25:1325–1335.
- Elmenhorst D, Kroll T, Matusch A, Bauer A. 2012. Sleep deprivation increases cerebral serotonin 2a receptor binding in humans. *Sleep*. 35:1615–1623.
- Fischl B, Sereno MI, Dale AM. 1999. Cortical surface-based analysis. *Neuroimage*. 9:195–207.
- Fischl B, Sereno MI, Tootell RBH, Dale AM. 1999. High-resolution inter-subject averaging and a surface-based coordinate system. *Hum Brain Mapp*. 8:272–284.
- Ganglbberger F, Kaczanowska J, Penninger JM, Hess A, Bühler K, Haubensak W. 2017. Predicting functional neuroanatomical maps from fusing brain networks with genetic information. *Neuroimage*. 170:113–120.
- Genovart N, Meyer JH, Boovariwala A, Hussey D, Rabiner EA, Houle S, Wilson AA. 2006. Positron emission tomography quantification of [11C]-harmine binding to monoamine oxidase-A in the human brain. *J Cereb Blood Flow Metab*. 26: 330–344.
- Glasser MF, Coalson TS, Robinson EC, Hacker CD, Harwell J, Yacoub E, Ugurbil K, Andersson J, Beckmann CF, Jenkinson M, et al. 2016. A multi-modal parcellation of human cerebral cortex. *Nature*. 536:171–178.
- Greve DN, Svarer C, Fisher PM, Feng L, Hansen AE, Baare W, Rosen B, Fischl B, Knudsen GM. 2014. Cortical surface-based analysis reduces bias and variance in kinetic modeling of brain PET data. *Neuroimage*. 92:225–236.
- Gryglewski G, Rischka L, Philippe C, Hahn A, James GM, Klebermass E, Hienert M, Silberbauer L, Vanicek T, Kautzky A, et al. 2017. Simple and rapid quantification of serotonin transporter binding using [11C]DASB bolus plus constant infusion. *Neuroimage*. 149:23–32.
- Gryglewski G, Seiger R, James GM, Godbersen GM, Komorowski A, Unterholzner J, Michenthaler P, Hahn A, Wadsak W, Mitterhauser M, et al. 2018. Spatial analysis and high resolution mapping of the human whole-brain transcriptome for integrative analysis in neuroimaging. 176:259–267.
- Horn DI, Yu C, Steiner J, Buchmann J, Kaufmann J, Osoba A, Eckert U, Zierhut KC, Schiltz K, He H, et al. 2010. Glutamatergic and resting-state functional connectivity correlates of severity in major depression - the role of pregenual anterior cingulate cortex and anterior insula. *Front Syst Neurosci*. 4:1–10.
- Ichise M, Liow JS, Lu JQ, Takano A, Model K, Toyama H, Suhara T, Suzuki K, Innis RB, Carson RE. 2003. Linearized reference tissue parametric imaging methods: application to [11C] DASB positron emission tomography studies of the serotonin transporter in human brain. *J Cereb Blood Flow Metab*. 23:1096–1112.
- Innis RB, Cunningham VJ, Delforge J, Fujita M, Gjedde A, Gunn RN, Holden J, Houle S, Huang SC, Ichise M, et al. 2007. Consensus nomenclature for in vivo imaging of reversibly binding radioligands. *J Cereb Blood Flow Metab*. 27: 1533–1539.
- James GM, Baldinger-Melich P, Philippe C, Kranz GS, Vanicek T, Hahn A, Gryglewski G, Hienert M, Spies M, Traub-Weidinger T, et al. 2017. Effects of selective serotonin reuptake

- inhibitors on interregional relation of serotonin transporter availability in major depression. *Front Hum Neurosci.* 11: 1–10.
- klumpers UMH, Veltman DJ, Drent ML, Boellaard R, Comans EFI, Meynen G, Lammertsma A a, Hoogendijk WJG. 2010. Reduced parahippocampal and lateral temporal GABA-[11C]flumazenil binding in major depression: preliminary results. *Eur J Nucl Med Mol Imaging.* 37:565–574.
- Knudsen GM, Jensen PS, Erritzoe D, Baare WF, Ettrup A, Fisher PM, Gillings N, Hansen HD, Hansen LK, Hasselbalch SG, et al. 2016. The Center for Integrated Molecular Brain Imaging (Cimbi) database. *Neuroimage.* 124:1213–1219.
- Kolbinger HM, Höflich G, Hufnagel A, Müller H-J, Kasper S. 1995. Transcranial magnetic stimulation (TMS) in the treatment of major depression—a pilot study. *Hum Psychopharmacol Clin Exp.* 10:305–310.
- Kraehenmann R, Preller KH, Scheidegger M, Pokorny T, Bosch OG, Seifritz E, Vollenweider FX. 2015. Psilocybin-induced decrease in amygdala reactivity correlates with enhanced positive mood in healthy volunteers. *Biol Psychiatry.* 78: 572–581.
- Landenberger R, Baldinger P, Hahn A, Ungersboeck J, Mitterhauser M, Winkler D, Micskei Z, Stein P, Karanikas G, Wadsak W, et al. 2013. Global decrease of serotonin-1A receptor binding after electroconvulsive therapy in major depression measured by PET. *Mol Psychiatry.* 18(1): 93–100.
- Landenberger R, Kranz GS, Haeusler D, Akimova E, Savli M, Hahn A, Mitterhauser M, Spindelegger C, Philippe C, Fink M, et al. 2012. Prediction of SSRI treatment response in major depression based on serotonin transporter interplay between median raphe nucleus and projection areas. *Neuroimage.* 63:874–881.
- Landenberger R, Mitterhauser M, Spindelegger C, Wadsak W, Klein N, Mien LK, Holik A, Attarbaschi T, Mossaheb N, Sacher J, et al. 2007. Reduced serotonin-1A receptor binding in social anxiety disorder. *Biol Psychiatry.* 61:1081–1089.
- Logan J, Fowler JS, Volkow ND, Wolf AP, Dewey SL, Schlyer DJ, MacGregor RR, Hitzemann R, Bendriem B, Gatley SJ, et al. 1990. Graphical analysis of reversible radioligand binding from time-activity measurements applied to [N-11C-methyl]-(-)-cocaine PET studies in human subjects. *J Cereb Blood Flow Metab.* 10:740–747.
- Martel JC, Leduc N, Ormière AM, Faucillon V, Danty N, Culie C, Cussac D, Newman-Tancredi A. 2007. WAY-100635 has high selectivity for serotonin 5-HT_{1A} versus dopamine D₄ receptors. *Eur J Pharmacol.* 574:15–19.
- Matsumoto M, Hidaka K, Tada S, Tasaki Y, Yamaguchi T. 1996. Low levels of mRNA for dopamine D₄ receptor in human cerebral cortex and striatum. *J Neurochem.* 66:915–919.
- Mayberg HS, Liotti M, Brannan SK, McGinnis S, Mahurin RK, Jerabek PA, Silva JA, Tekell JL, Martin CC, Lancaster JL, et al. 1999. Reciprocal limbic-cortical function and negative mood: converging PET findings in depression and normal sadness. *Am J Psychiatry.* 156:675–682.
- McCarthy CS, Ramprasad A, Thompson C, Botti JA, Coman IL, Kates WR. 2015. A comparison of FreeSurfer-generated data with and without manual intervention. *Front Neurosci.* 9:1–18.
- McKenna DJ, Towers GHN, Abbott F. 1984. Monoamine oxidase inhibitors in South American hallucinogenic plants: Tryptamine and β -carboline constituents of Ayahuasca. *J Ethnopharmacol.* 10:195–223.
- Mitchell JP, Heatherton TF, Macrae CN. 2013. Distinct neural systems subserve person and object knowledge. In: *Social Neuroscience: Key Readings.* New York (USA): Psychology Pres. p. 53–62.
- Montag C, Weber B, Fließbach K, Elger C, Reuter M. 2009. The BDNF Val66Met polymorphism impacts parahippocampal and amygdala volume in healthy humans: Incremental support for a genetic risk factor for depression. *Psychol Med.* 39: 1831–1839.
- Moreno-Dominguez D, Anwender A, Knösche TR. 2014. A hierarchical method for whole-brain connectivity-based parcellation. *Hum Brain Mapp.* 35:5000–5025.
- Parsey RV, Arango V, Olvet DM, Oquendo M a, Van Heertum RL, John Mann J. 2005. Regional heterogeneity of 5-HT_{1A} receptors in human cerebellum as assessed by positron emission tomography. *J Cereb Blood Flow Metab.* 25:785–793.
- Parsey RV, Kent JM, Oquendo MA, Richards MC, Pratap M, Cooper TB, Arango V, Mann JJ. 2006. Acute occupancy of brain serotonin transporter by sertraline as measured by [11C]DASB and positron emission tomography. *Biol Psychiatry.* 59:821–828.
- Parsey RV, Ogden RT, Miller JM, Tin A, Hesselgrave N, Goldstein E, Mikhno A, Milak M, Zanderigo F, Sullivan GM, et al. 2010. Higher serotonin 1A binding in a second major depression cohort: modeling and reference region considerations. *Biol Psychiatry.* 68:170–178.
- Pascual-Leone A, Rubio B, Pallardó F, Catalá MD. 1996. Rapid-rate transcranial magnetic stimulation of left dorsolateral prefrontal cortex in drug-resistant depression. *Lancet.* 348: 233–237.
- Paterson LM, Tyacke RJ, Nutt DJ, Knudsen GM. 2010. Measuring endogenous 5-HT release by emission tomography: promises and pitfalls. *J Cereb Blood Flow Metab.* 30:1682–1706.
- Power JD, Cohen AL, Nelson SM, Wig GS, Barnes KA, Church JA, Vogel AC, Laumann TO, Miezin FM, Schlaggar BL, et al. 2011. Functional network organization of the human brain. *Neuron.* 72:665–678.
- Raichle ME, Snyder AZ. 2007. A default mode of brain function: a brief history of an evolving idea. *Neuroimage.* 37: 1083–1090.
- Rousseeuw PJ. 1987. Silhouettes: a graphical aid to the interpretation and validation of cluster analysis. *J Comput Appl Math.* 20:53–65.
- Ruhe HG, van Rooijen G, Spijker J, Peeters FP, Schene AH. 2012. Staging methods for treatment resistant depression. A systematic review. *J Affect Disord.* 137:35–45.
- Sacher J, Rabiner EA, Clark M, Rusjan P, Soliman A, Boskovic R, Kish SJ, Wilson AA, Houle S, Meyer JH. 2012. Dynamic, adaptive changes in MAO-A binding after alterations in substrate availability: an in vivo 11C-harmine positron emission tomography study. *J Cereb Blood Flow Metab.* 32:443–446.
- Sartorius A, Demirakca T, Böhringer A, Clemm von Hohenberg C, Aksay SS, Bumb JM, Kranaster L, Ende G. 2016. Electroconvulsive therapy increases temporal gray matter volume and cortical thickness. *Eur Neuropsychopharmacol.* 26:506–517.
- Savli M, Bauer A, Mitterhauser M, Ding YS, Hahn A, Kroll T, Neumeister A, Haeusler D, Ungersboeck J, Henry S, et al. 2012. Normative database of the serotonergic system in healthy subjects using multi-tracer PET. *Neuroimage.* 63: 447–459.
- Schaefer A, Kong R, Gordon EM, Laumann TO, Zuo X-N, Holmes AJ, Eickhoff SB, Yeo BTT. 2017. Local-global parcellation of the human cerebral cortex from intrinsic functional connectivity MRI. *Cereb Cortex.* 28:1–20.
- Sheline YI, Barch DM, Price JL, Rundle MM, Vaishnavi SN, Snyder AZ, Mintun MA, Wang S, Coalson RS, Raichle ME.

2009. The default mode network and self-referential processes in depression. *Proc Natl Acad Sci USA*. 106:1942–1947.
- Spindelegger C, Lanzenberger R, Wadsak W, Mien LK, Stein P, Mitterhauser M, Moser U, Holik A, Pezawas L, Kletter K, et al. 2009. Influence of escitalopram treatment on 5-HT 1A receptor binding in limbic regions in patients with anxiety disorders. *Mol Psychiatry*. 14:1040–1050.
- Talairach J, Tournoux P. 1988. *Co-Planar Stereotaxis Atlas of the Human Brain*. Stuttgart (Germany): G. Thieme.
- Uylings HBM, Rajkowska G, Sanz-Arigita E, Amunts K, Zilles K. 2005. Consequences of large interindividual variability for human brain atlases: converging macroscopical imaging and microscopical neuroanatomy. *Anat Embryol (Berl)*. 210: 423–431.
- Van Essen DC. 2005. A Population-Average, Landmark- and Surface-based (PALS) atlas of human cerebral cortex. *Neuroimage*. 28:635–662.
- Vanicek T, Kutzelnigg A, Philippe C, Sigurdardottir HL, James GM, Hahn A, Kranz GS, Hoflich A, Kautzky A, Traub-Weidinger T, et al. 2017. Altered interregional molecular associations of the serotonin transporter in attention deficit/hyperactivity disorder assessed with PET. *Hum Brain Mapp*. 38:792–802.
- Varnas K, Halldin C, Hall H. 2004. Autoradiographic distribution of serotonin transporters and receptor subtypes in human brain. *Hum Brain Mapp*. 22:246–260.
- Vollenweider FX, Leenders KL, Scharfetter C, Maguire P, Stadelmann O, Angst J. 1997. Positron emission tomography and fluorodeoxyglucose studies of metabolic hyperfrontality and psychopathology in the psilocybin model of psychosis. *Neuropsychopharmacology*. 16:357–372.
- Yeo BTT, Krienen FM, Chee MWL, Buckner RL. 2014. Estimates of segregation and overlap of functional connectivity networks in the human cerebral cortex. *Neuroimage*. 88:212–227.
- Yeo BTT, Krienen FM, Sepulcre J, Sabuncu MR, Lashkari D, Hollinshead M, Roffman JL, Smoller JW, Zollei L, Polimeni JR, et al. 2011. The organization of the human cerebral cortex estimated by intrinsic functional connectivity. *J Neurophysiol*. 106:1125–1165.
- Zhu X, Wang X, Xiao J, Liao J, Zhong M, Wang W, Yao S. 2012. Evidence of a dissociation pattern in resting-state default mode network connectivity in first-episode, treatment-naive major depression patients. *Biol Psychiatry*. 71: 611–617.
- Zilles K, Amunts K. 2010. Centenary of Brodmann’s map conception and fate. *Nat Rev Neurosci*. 11:139–145.
- Zilles K, Palomero-Gallagher N, Grefkes C, Scheperjans F, Boy C, Amunts K, Schleicher A. 2002. Architectonics of the human cerebral cortex and transmitter receptor fingerprints: reconciling functional neuroanatomy and neurochemistry. *Eur Neuropsychopharmacol*. 12:587–599.